Available online at www.sciencedirect.com
SCIENCE DIRECT
Catalysis Today 107–108 (2005) 53–59
CATALYSIS TODAY
www.elsevier.com/locate/cattod

Preparation and characterization of Ce/Zr mixed oxides and their use as catalysts for the direct oxidation of dry CH_4

Susana Larrondo [a,*], María Adelina Vidal [a], Beatriz Irigoyen [a], Aldo F. Craievich [c], Diego G. Lamas [b], Ismael O. Fábregas [b], Gustavo E. Lascalea [b], Noemí E. Walsöe de Reca [b], Norma Amadeo [a]

[a] *Lab. de Procesos Catalíticos, Depto. de Ing. Química, Facultad de Ingeniería, University de Buenos Aires, Pab. de Industrias, Ciudad Universitaria, 1428 Buenos Aires, Argentina*
[b] *Centro de Investigaciones en Sólidos (CINSO), CITEFA-CONICET, J.B. de La Salle 4397, 1603 Villa Martelli, Buenos Aires, Argentina*
[c] *Instituto de Física, USP, Travessa R da Rua do Matão, no.187, Cidade Universitaria, 05508-900, São Paulo, SP, Brasil*

Available online 22 August 2005

Abstract

Solid oxide fuel cells have a promissory future in the direct combustion of fuels but, their main drawbacks are the high operation temperature and the rapid performance degradation due to carbon deposition in the anode. The development of ceria-based anodes with good electronic conductivity at lower temperatures seems to be a promising way to solve those problems.

In this work, preparation of compositionally homogeneous Ce/Zr oxides by a gel-combustion process and their characterization are reported. A detailed crystallographic study performed by synchrotron radiation X-ray diffraction has been carried out, in order to analyze the correlation between crystal structure and catalytic properties. The oxides presented specific area values, porous size distribution and carbon content values desirable for solid catalysts. Likewise, increasing the content of ZrO_2 facilitates the reducibility of both surface and bulk sites in the solid. The oxides have been active in the combustion of methane. Their performances were stable during a typical work period of 8 h, with no evidence of formation of carbonaceous deposits. The experiments were carried out confirm the promising features of these oxides as anodic materials in solid oxide fuel cells.

Keywords: Methane; Direct combustion; Ceria; Zirconia; Solid oxide fuel cell; SOFC

1. Introduction

In recent years, fuel cells have attracted much attention because they represent an alternative technology for power generation through the direct conversion of the chemical energy of the fuels in electrical energy [1]. Inside the fuel cell this conversion takes place in a much more efficient way than in the conventional heat engine systems limited by Carnot efficiency. Therefore, their application in power generation would lead to a better use of natural fossil fuels resources and a strong reduction of contaminant emissions [2].

Most of the work done in fuel cells is concerned with the use of hydrogen as fuel due to the mild characteristic of the oxidation product (water). Nevertheless, the main way to obtain hydrogen is by hydrocarbon steam reforming, which involves many reactors operating at different temperature conditions. The direct use of hydrocarbon in the fuel cell, without the necessity of reforming and purificating reactors, will improve the global efficiency of the system. In this sense, among several different types of fuel cells currently under development, solid oxide fuel cells (SOFCs) present the most promissory characteristics in the direct use of fuels. The operation principle of these cells involves the reduction of molecular oxygen in the cathode, the diffusion of oxygen anions through the electrolyte and the oxidation of the fuel by the oxygen anions in the anode [3]. This kind of cells has

* Corresponding author.
E-mail address: susana@di.fcen.uba.ar (S. Larrondo).

0920-5861/$ – see front matter © 2005 Elsevier B.V. All rights reserved.
doi:10.1016/j.cattod.2005.07.110

special advantages as environmentally friendly operation, higher fuel to electricity efficiency and fuel flexibility [4]. Nevertheless, they currently operate at temperatures around 900 °C, and this high operating temperature causes the degradation of electrodes, interfaces, and cell performance, and limits the choice of materials and fabrication methods, thus increasing the costs of the cell [5]. Then, substantial efforts have been done in order to reduce the operating temperature.

At present, ethanol and methane (or natural gas) are regarded as the most appropriate fuels to be used in SOFCs [6]: the first one, due to the natural availability of bioethanol and the second one, for its accessibility (natural gas) and physical properties.

Murray et al. [1] have studied the direct use of methane in fuel cells with ceria-based anodes. An important result presented by the authors was the stable direct oxidation of methane without carbon deposition in the Ni–YSZ–ceria anodes, at a temperature of 600 °C. They have pointed out that occurrence of carbon deposition by methane pyrolysis is not favored at temperatures lower than 700 °C, and carbon formation from CO disproportionation is not present at temperatures above 500 °C. Murray and Barnett [7] have observed the formation of carbonaceous deposits when using ethane as fuel in Ni-based anodes at temperatures as low as 500 °C. Many researchers have encountered that ceria-based anodes, with ceria doped with rare earth ions, are active and stable for the electrochemical oxidation of methane [8].

Then, a promissory strategy consists of developing ceria-based anodes with good electronic conductivity at lower temperatures through the doping with other oxides. This route has been examined by different research groups and the success in this direction will undoubtedly accelerate the commercial development of intermediate-temperature SOFCs of intermediate temperatures [2].

The objective of this work is to study the catalytic activity of nanocrystalline, compositionally homogeneous Ce/Zr mixed oxides for direct oxidation of methane, with the purpose of analyzing their possible use as anode materials in SOFCs. These mixed oxides were synthesized by a pH-controlled nitrate–citrate gel-combustion route and carefully characterized by several techniques.

It is worth to mention that the literature reports some work concerning the catalytic activity of Ce/Zr mixed oxides in the direct oxidation of methane. However, the most detailed work has been carried out for samples prepared by urea hydrolysis and coprecipitation methods [9,10], which may not result in compositionally homogeneous samples. This problem is evident in Ce/Zr mixed oxides synthesized by urea hydrolysis, since XRD diffraction data reported by Pengpanich et al. [9] clearly show a mixture of tetragonal and cubic phases for several compositions. In the case of the coprecipitated samples studied by Bozo et al. [10], even though X-ray diffraction data are not presented, the authors claimed that Zr is fully incorporated in the CeO_2 lattice. However, Rossignol et al. [11] clearly showed that Ce/Zr mixed oxides synthesized by these methods are not compositionally homogeneous, even for similar compositions and thermal treatments similar to those studied by Bozo and coworkers. Compositional homogeneity is a critical point in these materials, as it has been undoubtedly established by several authors. A practical criterion to verify the compositional homogeneity has been proposed by Fornasiero and coworkers [12–14]. These authors showed that compositional inhomogeneities may be revealed by X-ray diffraction analysis of powders calcined at 1000 °C for 5 h. Unfortunately, Bozo et al. did not use this criterion. On the other hand, the composition homogeneity of powders synthesized by pH-controlled nitrate–glycine gel-combustion process have been confirmed in previous work [15]. Therefore, the present study is of great importance for the understanding of the catalytic properties for methane oxidation of Ce/Zr mixed oxides.

In addition, in the present paper, a detailed crystallographic study was carried out by synchrotron radiation X-ray diffraction. This study was carried out in order to identify undoubtedly the crystal structure as a function of composition, which is very important to establish a correlation between crystal structure and catalytical properties. In fact, in the work of Bozo et al., the crystal structure was not analyzed, so this issue was not considered. Furthermore, recent works [14,16] suggested that compositional inhomogeneities may be present at a nanoscale level, being undetectable by conventional X-ray diffraction. The use of synchrotron radiation coupled with the experimental configuration employed in this work provides a very intense X-ray beam, which is very useful to reveal these nanoscale heterogeneities.

2. Experimental

2.1. Catalyst preparation

CeO_2 powders with 10, 30 and 50 mol% of ZrO_2, were synthesized by pH-controlled nitrate–glycine gel-combustion process described in a previous work [15]. $ZrOCl_2{\cdot}8H_2O$ and $Ce(NO_3)_3{\cdot}6H_2O$ solids were dissolved in nitric acid in a ratio corresponding to the desired final composition and this solution was concentrated by thermal evaporation in order to eliminate chloride anions. Glycine was added in a proportion 5 mol of glycine per mole of metal atom and the pH of the solution was adjusted to pH 7 with ammonium hydroxide. The resulting solution was concentrated on a hot plate at 200 °C until a viscous gel was obtained, which finally burned due to a vigorous exothermic reaction. The as-reacted material was then calcined in air for 2 h in order to eliminate carbonaceous residues. Samples were calcined at two different calcination temperatures, 600 and 800 °C, in order to see the effect in the pore volume, crystal diameter and specific surface.

For identification purpose, samples received a denomination formed by letter Z, from zirconia, followed by the first number of zirconia mol% and the first number of calcination temperature. Thus, sample Z16 represents a sample with 10 mol% of ZrO_2 that was calcined at 600 °C, while sample Z18 represents a sample with 10 mol% of ZrO_2 that was calcined at 800 °C.

2.2. Sortometry

The specific surface was determined from the N_2 adsorption isotherm at its normal boiling temperature (−196 °C), by the Brunauer, Emmett and Teller (BET) method. Sortometry was performed in the Gemini 2360 Micromeritics automatic equipment that reports the BET specific surface and total pore volume. Samples were previously degassed in the FlowPrep 060 Degasser, with helium at temperature of 117 °C for 2 h.

Micropore volume was estimated by the Dubinin–Radushkevitch (D–R) equation [17]

$$\log V_a = \log V_o - \frac{k \times 2.303 R^2 T^2}{\beta^2} \left[\log\left(\frac{p_o}{p}\right)\right]^2$$

where V_o represents the micro-pore total volume, V_a the pore total volume, k a parameter that characterizes pore size distribution and β is the affinity coefficient. The results obtained from N_2 adsorption were plotted as $\log V_a$ versus $[\log(p/p_o)]^2$. The function was approximated by linear regression and V_o was obtained from the ordinate at origin.

2.3. Synchrotron radiation X-ray diffraction (SR-XRD)

Synchrotron radiation X-ray diffraction experiments were carried out at XRD-1 beamline of the Brazilian Synchrotron Light Laboratory (LNLS, Campinas, Brazil). In order to detect the weak 112 reflection of the tetragonal solid solutions, a high-intensity (low-resolution) configuration, without crystal analyzer, was employed. In this way, it was possible to increase the signal-to-noise ratio significantly. The wavelength was set as 1.50006 Å. Data in the angular region of $2\theta = 20$–130° were collected in a step-scanning mode, with a step length of 0.04° and a step-counting time of 2 s. The 2θ region close to the (1 1 2) peak was analyzed with larger step-counting times. The crystallite size was determined by means of the Scherrer equation.

SR-XRD data were analyzed by the Rietveld method using the program FullProf. The $P4_2/nmc$ space group was assumed with (Zr^{4+}, Ce^{4+}) cations and O^{2-} anions in 2a and 4d positions, respectively. The lattice parameters, a and c, and the fractional z coordinate of the O^{2-} anion in the tetragonal asymmetric unit, $z(O)$, were refined. The results of these refinements will be expressed in terms of the usual pseudo-fluorite unit cell. The peak shape was assumed to be a pseudo-Voigt function. The background of each profile was adjusted by a six-parameter polynomial function in $(2\theta)^n$, $n = 0$–5. Isotropic atomic thermal parameters were used. For powders with a composition of ZrO_2–90 mol% CeO_2, the above $P4_2/nmc$ structural model was compared with the fluorite one: $Fm\bar{3}m$ space group with (Zr^{4+}, Ce^{4+}) cations and O^{2-} anions in 4a and 8c positions, respectively.

2.4. CHN Elemental analysis

The solids were prepared by a gel-combustion method that could leave carbonaceous deposits on their surface. In order to determine the carbon content after the calcination procedure, elemental CHN analysis were performed.

The experiments were carried out in an elemental analyzer EA1108El, designed for the micro, semi-micro and macro determination of total carbon, hydrogen and nitrogen. The analytical method is based on the complete and instantaneous oxidation of the sample by ''flash combustion'', which converts all organic and inorganic substances into combustion products. The resulting combustion gases pass through a reduction furnace and are swept into the chromatographic column by the carrier gas (helium) where they are separated and detected by a thermal conductivity detector (TCD).

2.5. Temperature programmed reduction (TPR)

TPR experiments were performed in conventional laboratory equipment, with temperature programmer and controller, and hydrogen as reduction agent. The rate of hydrogen consumption was detected by a thermal conductivity detector placed in an isothermal oil bath. The detector signal was digitized and saved in a computer.

Before reduction, solid samples were dried at 110 °C until getting a constant mass of 100 mg. A gas mixture of 4.5 mol% of H_2 and 98 mol% of N_2, with a total flow of 115 cm^3 NPTC min^{-1} was used. The temperature was raised from 100 °C to 1000 °C at a rate of 10 °C min^{-1}. Conditions selected to perform the analysis follow the recommendations reported in references [18] and [19] for this technique.

2.6. Catalytic tests

Catalytic tests were carried out in a conventional fixed-bed flow reactor, operated isothermally at atmospheric pressure. The reactor was made with a stainless steel tube of 9.96 mm inner diameter. The reactor was heated with an electric oven equipped with temperature controller. The reaction temperature was measured with a thermocouple placed inside the catalytic bed. The feed consisted of a mixture of 1 mol% CH_4, 4 mol% O_2 and N_2 balance, with total flow of 229 cm^3 NPTC min^{-1}, kept constant by mass-flow controllers. Feed composition was checked and effluent composition was determined using on-line gas chromatography, in a HP 6890+ gas chromatograph, equipped with a TCD and a CTR1 of 6 ft × 1/4 in. column (concentric

column, tube type, molecular sieve 5A and Porapak Q) and automatic injection valve.

Catalyst mass was 90 mg in all experiments. Since methane oxidation is highly exothermal, the catalytic bed was diluted with inter particles in a 20/1 mass ratio, in order to avoid adverse thermal effects.

Methane conversion was calculated as (moles of methane converted/mole of methane fed) in the time unit.

The reactor was operated in steady state within the following operating conditions: catalyst mass: 90 mg; total feed rate: 229 cm^3 NPTC min^{-1}: methane molar fraction: 0.01; oxygen molar fraction: 0.04; nitrogen balance; temperature range: 450–850 °C.

Previous catalytic tests were performed in order to ensure that, at the selected operating conditions, there was a negligible contribution of homogeneous oxidation to total conversion and there were no internal and external diffusion limitations. The catalysts showed activity without the necessity of a pretreatment and their performances were stable during a typical run period of 8 h.

3. Results and discussion

The results obtained in sortometry experiments have been summarized in Table 1. It can be seen that the specific area values are almost the same with the exception of sample Z36. In addition, there is an increment in total pore volume with a decrease in zirconia content. Besides, micro-pore volume is practically constant. This leads to the conclusion that samples Z16 and Z18 have a higher proportion of meso-pores in their structures. Likewise, an influence of the calcination temperature in pore volume and specific area values has not been observed.

In Fig. 1, the diffractograms of Z16, Z36 and Z56 are presented in a logarithmic scale. Fig. 2 shows the 2θ regions corresponding to the (4 0 0) and (0 0 4) reflections. As it can be observed, the Z56 sample exhibits a small splitting of these peaks, while only one peak can be observed for Z16 and Z36 samples. Fig. 3 shows the region around the (1 1 2) peak, which is related to the displacement of the oxygen anions. It can be observed that Z36 and Z56 powders exhibit this peak (which is very small for the Z36 sample), while it is not observed in the case of the Z16 powder. These results

Table 1
Sortometry results: specific area and total pore volume of fresh catalyst

Sample	Specific area (m^2/g)	Pore volume (cm^3/g)	Micro-pore volume (cm^3/g)
Z58	31	0.034	0.015
Z56	28	0.034	0.015
Z38	30	0.030	0.015
Z36	60	0.053	0.014
Z18	28	0.088	0.015
Z16	28	0.067	0.016

Total micro-pore volume calculated by R–D equation.

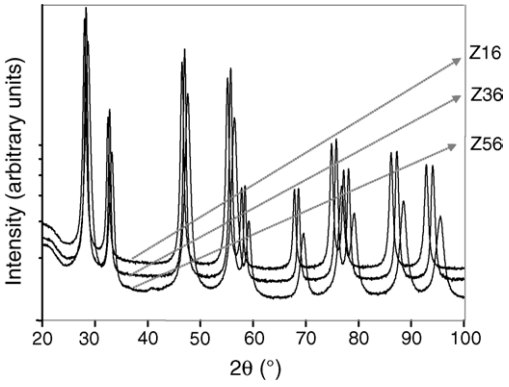

Fig. 1. SR-XRD data of powders calcined at 600 °C.

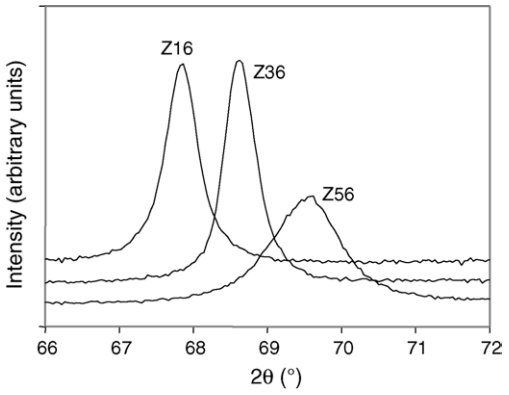

Fig. 2. SR-XRD data of powders calcined at 600 °C, for the 2θ region corresponding to the (0 0 4) and (4 0 0) reflections.

indicate that the Z56 powder exhibits the t′-form of the tetragonal phase, the Z36 powder exhibits the t″-form of the tetragonal phase and the Z16 powder exhibits the cubic phase. Table 2 summarizes the results obtained by Rietveld refinements, which confirm the above qualitative analysis.

The crystallite size determined by the Scherrer equation was in the range of 13–16 nm for all the powders calcined at 600 °C, while those calcined at 800 °C presented crystallite sizes in the range of 25–30 nm.

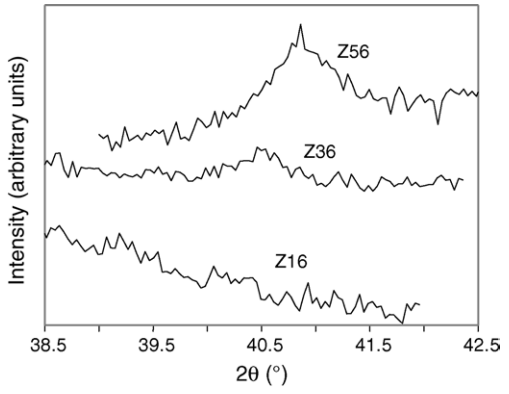

Fig. 3. SR-XRD data of powders calcined at 600 °C, for the 2θ region corresponding to the (1 1 2) reflection.

Table 2
Structural parameters and standard Rietveld agreement factors obtained for the nanocrystalline ZrO_2–CeO_2 powders calcined at 600 °C

	Z56 $P4_2/nmc$	Z36 $P4_2/nmc$	Z16 $Fm\bar{3}m$
a (Å)	5.26243 (1)	5.32770 (6)	5.38240 (5)
c (Å)	5.2873 (2)	5.32770 (6)	
c/a	1.00473 (6)	1	1
$z(O)$	0.222 (1)	0.241 (4)	0.25
B(Zr, Ce) (Å^2)	0.54 (1)	0.25 (1)	0.19 (1)
B(O) (Å^2)	1.29 (7)	0.91 (7)	0.72 (3)
R_p	4.03	5.21	3.81
R_{wp}	5.15	4.83	3.51
R_{exp}	1.30	1.49	1.55
χ^2	15.67	10.52	5.14

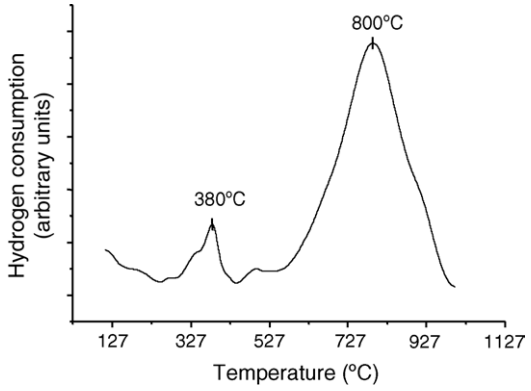

Fig. 4. TPR profile of CeO_2.

As it was mentioned in the introduction, Mamontov et al. found nanoscale heterogeneities for materials synthesized by different methods. These authors analyzed nanocrystalline powders of $Ce_{0.5}Zr_{0.5}O_2$ and found that the nanocrystallites consists of nanodomains of $Ce_{0.4}Zr_{0.6}O_2$ composition of 25–30 Å in size, in a matrix of $Ce_{0.7}Zr_{0.3}O_2$. According to this description, weak and very broad peaks corresponding to the nanodomains should be observed at 2θ-positions displaced from those of the matrix. If both compositions are very different, as reported by Mamontov et al., these broad peaks should be clearly observed at high angles. In addition, they could also modify the profile of the low-angle peaks, even for a smaller difference in composition. Therefore, the presence of these nanodomains should be detected by analyzing the peak shape. However, in spite of the high intensity of the X-ray beam used in this work, these effects, with such broad peaks have not been observed. Therefore, powders synthesized by gel-combustion seem to be compositionally homogeneous even at a nanoscale level [16].

In Table 3, the results from CHN analysis are presented. The carbon and hydrogen content is similar for all the solids, while nitrogen content is much lower for samples Z16 and Z18. Nevertheless, all the % (m/m) values have been low enough to conclude that the carbon formed during catalyst preparation, at the gel-combustion step, has been eliminated in the calcination process.

Ce-based oxides can store oxygen when they are in contact with an oxidant atmosphere, and release oxygen when they are in the presence of a reductive atmosphere. This process is sustained by the C^{4+}/Ce^{3+} redox couple. Then, the reduction profile of the solid in a H_2 atmosphere is tightly related with that redox process and with the feasibility of oxygen release. In Fig. 4, TPR profile of CeO_2 is presented. It can be noticed that the reduction of the pure oxide has taken place in two stages [20]. Peak maxima are placed at 380 °C and 800 °C, respectively. The results are similar to those reported by other authors [21]. The first peak is involved in the reduction of surface sites while the second peak in bulk sites.

For Ce/Zr mixed oxides the TPR results are presented in Table 4. Comparing the results presented in Table 4 to the same Zr content it is possible to conclude that calcination temperature slightly moves TPR profiles at higher temperatures. On the contrary, a strong effect of Zr content is observed. Comparing peak positions in Fig. 4 with the results presented in Table 4, it is possible to conclude that the peak appearing at 380 °C on CeO_2 strongly shifted to lower temperatures in Ce/Zr solids, indicating that the reduction of surface sites was highly enhanced. A similar conclusion could be achieved comparing the position of peak appearing at 800 °C on CeO_2 with the signals at higher temperature in Ce/Zr samples, concluding that Zr not only enhances the reduction of surface sites but also the reduction of bulk sites. Thus, the presence of Zr in the solid structure has strongly improved the reducibility of both surface and bulk ceria sites. These results are very important because they differ from those previously reported by other authors. Bouzo et al. [10] have observed a shifting of the first peak of TPR profile to higher temperatures, and an increment in H_2 consumption as Zr is incorporated in the structure, concluding that more Ce sites are reduced by hydrogen with the incorporation of Zr cations, while we have found that Ce is reduced more easily (at lower temepratures) as Zr is incorporated in the structure. Pengpanich et al. [9] have presented the CO-TPR

Table 3
C, H and N contents determined by elemental analysis

Sample	C (%, m/m)	H (%, m/m)	N (%, m/m)
Z58	0.292	0.060	0.307
Z56	0.198	0.053	0.310
Z38	0.231	0.070	0.517
Z36	0.296	0.073	0.557
Z18	0.204	0.067	0.019
Z16	0.266	0.110	0.059

Table 4
Peak temperatures from H_2 TPR profiles

	Z56 (°C)	Z36 (°C)	Z16 (°C)	Z58 (°C)	Z38 (°C)	Z18 (°C)
T1	187	181	108	194	247	197
T2	–	–	472	–	–	494
T3	569	530	719	582	597	747

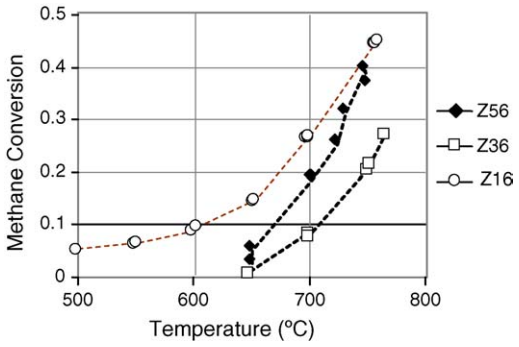

Fig. 5. Methane conversion vs. reaction temperature. For samples calcined at 600 °C.

results for Ce/Zr mixed oxides. They have also observed a similar TPR profile for CeO_2 and $Ce_{0.75}Zr_{0.25}O_2$ and a movement of TPR peaks to higher temperatures for higher Zr incorporation.

Another important result is the third TPR peak, labeled as T2 in Table 4, which we have observed for samples with 10 mol% of zirconia, Z16 and Z18. These signals correspond to bulk centers of intermediate reducibility that could release oxygen more easily and would play an important role in oxidation reactions.

The methane conversion as a function of the reaction temperature is plotted in Figs. 5 and 6. The results for solids calcined at 600 °C are presented in Fig. 5, while the results for samples calcined at 800 °C are presented in Fig. 6. Methane conversions at 500 °C for catalysts Z16 and Z18 are 0.05 and 0.13, respectively, and neglectable for samples Z36, Z56, Z38 and Z58. Conversions for the latter become important at higher temperatures. At this point it is important to remark that the products formed, at the operating conditions used in this work, were carbon dioxide and water, and a good carbon balance was obtained between reactor inlet and outlet. Then, formation of carbonaceous deposits is dismissed.

Catalysts with 10% of Zr have higher values of methane conversion than the other samples in all the temperature range used in the experiments. The different behavior cannot be related to the specific area because, as indicated above, all samples have similar values of this parameter. On the other side, the TPR results for solids Z16 and Z18 have shown a third peak at intermediate temperature, suggesting the existence of more labile oxygen ions in the structures that would oxidize methane more easily. At 600 °C, the best methane conversion we have report here is 20%, which is in the range of 10–80% reported by Pengpanich et al. [9] and lower than the 50% reported by Bozo et al. [10]. Nevertheless, it is important to remark that we have tested the solids at a space-time (catalyst mass/feed flow) 3 times lower than that used by Pengpanich et al. [9] and 12.5 times lower than that used by Bozo et al. [10]. Then, our solids could be potentially more active than those prepared by other methods [9–10] and to perform a deep kinetic study could be of great interest.

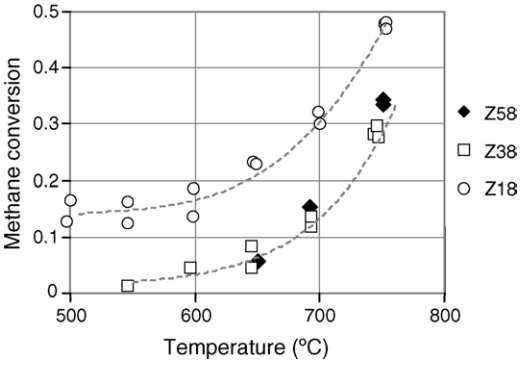

Fig. 6. Methane conversion vs. reaction temperature. For samples calcined at 800 °C.

Comparing the results plotted in Figs. 5 and 6 it is possible to say that solid Z18 has better performance than Sample Z16.

Then, it would be interesting to study the behavior of solid Z18 as catalysts in methane oxidation reaction, at different contact times, temperatures and feed composition, and its further evaluation as anode material in one-chamber solid oxide fuel cells with dry methane as feed.

4. Conclusions

Compositionally homogeneous CeO_2/ZrO_2 solids with values of specific areas and pore distribution appropriate for their use as catalysts have been prepared by the gel-combustion method. Calcination temperature has shown no incidence on solids textural-properties. Low carbon contents have been observed in fresh samples, indicating that carbon deposits formed during the gel-combustion step were satisfactorily removed in the calcination process.

The reducibility of the solids associated with both surface and bulk cerium sites has been facilitated by ZrO_2. Besides, increments in ZrO_2 content have produced changes in the solid structure from the cubic form of CeO_2 to the tetragonal one for ZrO_2.

At the operating conditions used in the present work, all the solids have shown activity for the combustion of methane at temperatures below 800 °C, without the necessity of a pretreatment. Their performances were stable during a work period of 8 h, without formation of carbon deposits. The reaction products have only produced carbon dioxide and water and a good carbon balance between reactor inlet and outlet has been observed. All these characteristics make it interesting for these solids to be studied as possible materials for anodes of SOFCs. Among them, solids with 10% of Zr, either calcined at 600 or 800 °C, which present centers with intermediate reducibility and better activity, are the more promising one.

Nevertheless, in order to clearly establish the correlation between the catalytic performances and the structural

features of the different studied samples, additional investigation is needed.

Acknowledgements

Authors wish to thank Mr. Roberto Tejeda for the TPR measurements, Mr. Eduardo Granado and Mr. Roosevelt Droppa, for their help during XRD experiments carried out at the XRD-1 beamline of the LNLS.

Synchrotron radiation X-ray diffraction experiments were performed in the frame of the scientific collaboration agreement between CAPES (Brazil) and SECyT (Argentina).

The financial support of Universidad de Buenos Aires (projects UBACyT I608 and I020), Agencia Nacional de Promoción Científica y Tecnológica (Argentina, PICT No. 8688), Fundación YPF (Repsol YPF Prize 2003) and LNLS (proposal D12A–XRD1–1857) is gratefully acknowledged.

References

[1] E.P. Murray, T. Tsai, S.A. Barnett, Nature 400 (1999) 649.
[2] B.C.H. Steele, Nature 400 (1999) 619.
[3] S. Park, R.J. Gorte, J.M. Vohs, Appl. Catal. A 200 (2000) 55.
[4] S.P.S. Badwal, K. Foger, Ceram. Int. 22 (1996) 257.
[5] S.H. Clarke, A.L. Kicks, K. Pointon, T.A. Smith, A. Swann, Catal. Today 38:4 (1997) 411.
[6] S.L. Douvartzides, F.A. Coutelieris, A.K. Demin, P.E. Tsiakaras, AIChE J. 49 (2003) 248.
[7] E.P. Murray, S.A. Barnett, in: S.C. Singhal, M. Dokiya (Eds.), Proceeding of the Sixth International Symposium on Solid Oxide Fuel Cells, SOFC VI, The Electrochemical Society, Pennington, NJ, 1999, p. 1001.
[8] M. Ahibzada, B.C.H. Steele, K. Zheng, R.A. Rudkin, I.S. Metcalfe, Catal. Today 38 (1997) 1001.
[9] S. Pengpanich, V. Meeyoo, T. Rirksomboon, K. Bunyakiat, Appl. Catal. A 234 (2002) 221.
[10] C. Bozo, N. Guilhaume, E. Garbowski, M. Primet, Catal. Today 59 (2000) 33.
[11] S. Rossignol, F. Gérard, D. Duprez, J. Mater. Chem. 9 (1999) 1615.
[12] P. Fornasiero, E. Fonda, R. Di Monte, G. Vlaic, J. Kaspar, M. Graziani, J. Catal. 187 (1999) 177.
[13] J. Kaspar, P. Fornasiero, in: A. Trovarelli (Ed.), Catalysis by Ceria and Related Materials, Imperial College Press, London, 2002, p. 217.
[14] R. Di Monte, J. Kaspar, J. Mater. Chem. 15 (2005) 633.
[15] D.G. Lamas, G.E. Lascalea, R.E.J. Juárez, E. Djurado, L. Pérez, N.E. Walsöe de Reca, J. Mater. Chem. 13 (2003) 904.
[16] E. Mamontov, R. Brezny, M. Koranne, T. Egami, J. Phys. Chem. B 107 (2003) 13007.
[17] S.J. Gregg, K.S.W. Sing, Adsorption Surface Area and Porosity, Academic Press Inc., London, 1982.
[18] D.A. Monti, A. Baiker, J. Catal. 83 (1983) 323.
[19] P. Malet, A. Caballero, J. Chem. Soc. Faraday Trans. 84 (1988) 2369.
[20] D.G. Lamas, G.E. Lascalea, M.D. Cabezas, R.O. Fuentes, I.O. Fábregas, M.E. Fernández de Rapp, N.E. Walsöe de Reca, S. Larrondo, R. Tejeda, N. Amadeo, Actas de las Jornadas SAM/CONAMET/SIMPOSIO MATERIA, 2003, p. 1030.
[21] A. Trovarelli, Catal. Rev. Sci. Eng. 38 (4) (1996) 439.